Dynamics of Filamentous Viruses in

Polyelectrolyte Solutions

Farshad Safi Samghabadi,[†] Ali H. Slim,[†] Maxwell W. Smith,[†] Maede Chabi,[‡] and Jacinta C. Conrad*,[†]

†Department of Chemical and Biomolecular Engineering, University of Houston, Houston,
Texas 77204, United States

‡Department of Biomedical Engineering, University of Houston, Houston, Texas 77204,

United States

E-mail: jcconrad@uh.edu

Abstract

The structure and dynamics of polyelectrolytes differ from those of neutral polymers. How these differences affect the transport of anisotropic particles remains incompletely understood. Here, we investigate the transport of semiflexible M13 bacteriophage (phage) in aqueous semidilute solutions of sodium polystyrene sulfonate (PSS) with various ionic strengths using fluorescence microscopy. We tune the characteristic length scales of the PSS using two molecular weights of 68 and 2200 kDa and by varying the ionic strength of the solutions from 10^{-6} to 10^{-1} M. Phage exhibit diffusive dynamics across all polymer concentrations. For 2200 kDa PSS solutions, the phage dynamics monotonically deviate from the bulk prediction as polymer concentration increases and exhibit non-Gaussian distributions of displacements. Existing scaling theories can approximately collapse dynamics as a function of phage hydrodynamic radius to polymer size ratio $R_{\rm h}/\xi$ onto a master curve across polymer concentrations

and ionic strengths. This partial collapse, however, does not follow the prediction for diffusion of isotropic particles in flexible Gaussian chains, suggesting the presence of multiple diffusive modes due to the anisotropic structure of the phage and the confining length scales set by the structure and dynamics of charged polymers.

Introduction

Phage are viruses that can infect, and in many cases, kill bacteria without harming plant or animal cells. The inherent properties of these virions along with their unique structural features make them promising agents in applications such as phage display, ^{1,2} drug and vaccine delivery, ^{3,4} therapy for multidrug-resistant bacterial infections, ^{5,6} and biorecognition processes. ⁷ The performance of phage is controlled by their transport properties in polymeric complex fluids such as mucus and the extracellular matrix. Thus, understanding the mechanisms that control phage diffusion in macromolecular fluids is essential to enhancing the efficacy of phage used in each of these applications.

The diffusion of a sphere of radius $R_{\rm NP}$ in a continuous medium with viscosity η is given by the Stokes-Einstein (SE) relationship, $D_{\rm SE} = k_{\rm B}T/6\pi\eta R_{\rm NP}$. This relationship has been extended to predict the diffusivity of nanorods by incorporating the anisotropy of the particles.⁸ The continuum assumption underlying the SE model fails, however, when the particle and polymer length scales become comparable, resulting in deviations from the SE predictions for both isotropic ⁹⁻¹⁶ and anisotropic ¹⁷⁻²¹ particles. In this size range, particle dynamics are controlled by the relative size of particle and polymer. In entangled polymer systems, the controlling length scale of the particle dynamics is the tube diameter $d_{\rm t}$, the mesh size of the entanglements. Whereas diffusion of particles much smaller than the tube diameter is unaffected by the polymer network, transport of large particles is dictated by chain entanglements that relax through reptation. ²²⁻²⁵ In unentangled solutions, however, particle dynamics are controlled by the polymer correlation length ξ , the average distance between neighboring chains. These length scales have served as the basis of models and

theories to predict the dynamics of nanoparticles.

Models predicting particle-polymer dynamics often use obstruction, ^{26,27} hydrodynamic, ^{28–30} or free volume³¹ approaches to describe the effects of the characteristic length scales on particle diffusion. More recently, a scaling model extended hydrodynamic theories to account for the coupling between the dynamics of particles and polymer chains.³² These models, however, are developed for diffusion of isotropic particles in neutral polymers. Anisotropic particles, unlike spheres, are characterized by anisotropic hydrodynamic friction coefficients that generate multiple diffusive modes. 33,34 Moreover, charged polymers have unique structural properties compared to neutral polymers. 35,36 Electrostatic interactions along the polymer backbone, determined by the number, size, and location of the charged groups within the monomers, change the chain structure and flexibility.^{37–41} In uncharged polymer solutions above the overlap concentration, the rotational and translational diffusivity of rodlike viruses fall below and above the SE prediction, respectively, suggesting the onset of topological constraints that affect the rotational and translational motion of these nanoparticles to different extents. 17,42 Moreover, diffusion of viruses with different aspect ratios and flexibility in partially hydrolyzed semidilute polymer solutions is controlled by a length scale that is intermediate between the virus radius and length. 43 Both the presence of multiple characteristic length scales in anisotropic particles and differences in chain dynamics and relaxations in charged polymers likely affect the length scales controlling the diffusive transport of particles. Despite recent studies about the transport of anisotropic particles in polymer liquids, $^{17,18,21,43-46}$ how the dynamics of these particles couple to dynamics of charged polymers remains incompletely understood.

Here, we study the dynamics of semiflexible, filamentous M13 phage in aqueous semidilute solutions of sodium poly(styrene sulfonate) (PSS) using fluorescence microscopy. The polymer conformation is tuned by varying the concentration and ionic strength of the solutions. Phage exhibit diffusive dynamics that are faster than nanospheres of equivalent hydrodynamic size. We find that in low molecular weight PSS solutions, phage dynamics follow

the predictions for the diffusivity of rods based on the bulk viscosity at all ionic strengths. The diffusivity of phage in solutions of high molecular weight PSS, however, deviates from the bulk prediction concomitant with concentration. The size-dependent phage dynamics can approximately be collapsed onto a master curve as a ratio of the phage hydrodynamic radius R_h and polymer correlation length ξ , albeit with a different scaling exponent than that predicted for diffusion of isotropic particles in Gaussian chains.

Materials and methods

Viral and spherical nanoparticles

Filamentous bacteriophage M13 (Guild Biosciences) with length of L=900 nm and diameter of 2R=6 nm were used as anisotropic probes. M13 is a semiflexible virus with the ratio of persistence length $L_{\rm p}\approx 2000$ nm and contour length L of $L/L_{\rm p}\approx 0.45$. These viral nanoparticles were fluorescently labeled with Alexa Fluor 555 (NHS ester, Thermo Fisher Scientific; peak excitation and emission at 488 and 532 nm, respectively). Prior to fluorescent labeling, the virus stock was buffer-exchanged from storage buffer to 0.2 M sodium bicarbonate buffer at pH 8.3 using a Zeba column (7 kDa MWCO; Thermo Fisher Scientific). Next, 100 μ L of the virus stock was mixed with 10 μ L of the dye solution (10 mg mL⁻¹ Alexa Fluor 555 in dimethyl sulfoxide) and incubated overnight at 4°C. To remove unreacted dye molecules, the virus-dye solution was washed three times with a centrifugal filter unit (Amicon Ultra-15, 100 kDa MWCO; Sigma Aldrich) at 4000g for 20 minutes. Finally, the labeled viruses were transferred to a storage tube, covered in aluminum foil, and stored in the refrigerator until used. Fluorescent polystyrene (PS) nanospheres of radius 100 nm (Fluoro-Max, Thermo Fisher Scientific) were used as control probes.

Solution preparation

Semidilute solutions of sodium polystyrene sulfonate (PSS) with weight-averaged molecular weights $M_{\rm w}$ of 2200 and 68 kDa (Scientific Polymer Products) were prepared at various concentrations and ionic strengths. To remove any excess salt, glass vials were cleaned by soaking overnight in a solution of potassium hydroxide in isopropanol, rinsed multiple times with Millipore water, and subsequently dried in a convection oven. Near salt-free aqueous solutions prepared using deionized (DI) water were assumed to have an ionic strength of 10^{-6} M. $^{48-50}$ Solutions with ionic strengths of 10^{-3} , 10^{-2} , and 10^{-1} M were prepared using sodium chloride without added buffer. To ensure that the polymer solutions were homogenized, samples were mixed for at least 24 h on a roll mill. The overlap concentration c^* of the PSS was estimated as the inverse of the intrinsic viscosity $c^* = 1/[\eta]$ measured using an Ubbelohde viscometer (Fig. S1, Supporting Information). The radius of gyration of a polymer at a given ionic strength was then calculated using $R_{\rm g,0}=(M_w[\eta]/\frac{4}{3}\pi N_{\rm av})^{1/3}$ where $N_{\rm av}$ is Avogadro's number (Table S1, Supporting Information). To avoid aggregation and non-uniform particle dispersion in low molecular weight PSS solutions, the M13 phage stock solution was diluted 50x with 0.2 M NaCl. Nanoparticles (viruses or nanospheres) at volume fraction of $\phi = 5 \times 10^{-4}$ were added to the polymer solution immediately prior to the imaging experiments.

Bulk rheology

A Discovery Hybrid Rheometer (HR-2, TA Instruments) equipped with a Couette geometry (cup diameter of 15 mm, bob diameter of 14 mm, and bob length of 42 mm) was used to measure the viscosity of the semidilute polymer solutions as a function of shear rate at 20°C. 10 ml of the polymer solution was gently loaded into the cell by contacting the pipette tip to the cell wall to avoid bubble formation in the sample. At each shear rate, the solution was presheared for 1 min to reach equilibrium and data were collected over the next 30 s. The instrument was calibrated for inertia and torque before each measurement.

Imaging and tracking

Air-tight chambers for imaging were assembled using coverslips (Fisherbrand cover glass) that were adhered on a glass microscope slide (Gold Seal Cover Glass; Thermo Fisher Scientific). The sample solution was pipetted into the chamber and sealed with UV epoxy-based adhesive (Norland Products) to prevent microscopic motion. Viruses and nanospheres in polymer solutions were imaged using a TCS SP8 confocal mounted on an inverted DMi8 microscope (Leica Microsystems) that was equipped with a 63x (N.A. 1.4) oil immersion lens. For each sample, four series of 4000 images at different locations were acquired with a pixel size of 163 nm at a rate of 28 frames per second. Using particle-tracking algorithms, ⁵¹ the centroids of the particles were identified, located, and linked to obtain particle trajectories over time. From the trajectories of the nanoparticles, we calculated the one-dimensional ensemble averaged mean-squared displacement (MSD) $\langle \Delta x^2 \rangle = \langle (x(t +$ $(\Delta t) - x(t)^2$, where x(t) is the x-position of the particle at time t and (Δt) is the lag time. Each data point in the MSD was averaged over at least 10⁴ time steps. Then, the diffusion coefficient was extracted from a linear fit of MSD = $2D\Delta t$. We also calculated the probability distribution of displacements (PDD), which measures the probability of particles displacing a distance Δx at a lag time Δt , via the self-part of the van Hove function $G_s(\Delta x, \Delta t) = \frac{1}{N} \left\langle \sum_{i=1}^{N} \delta((x_i(t) - x_i(t + \Delta t) - \Delta x)) \right\rangle$. Finally, we calculated the non-Gaussian parameter $\alpha_2 = [\langle \Delta x^4 \rangle/3 \langle \Delta x^2 \rangle^2] - 1$ and ergodicity breaking parameter ter EB = $[\langle (\delta x^2)^2 \rangle - \langle \Delta x^2 \rangle^2] / \langle \Delta x^2 \rangle^2$, where δx^2 is the individual time-averaged squared displacement of each trajectory.

Results and discussion

The rheological properties of semidilute solutions of charged polymers depend on ionic strength, in contrast to those of neutral polymers. ^{36,52} The specific viscosity $\eta_{\rm sp} = (\eta - \eta_{\rm s})/\eta_{\rm s}$, where η and $\eta_{\rm s}$ are the solution and solvent viscosities, respectively, is a measure of the poly-

mer contribution to the solution viscosity. For solutions of 2200 kDa PSS, $\eta_{\rm sp}$ increases as concentration and ionic strength are increased (Fig. 1). For $c < c^*$, due to the dominance of the hydrodynamic forces, the specific viscosity is independent of the ionic strength and scales with polymer concentration as $\eta_{\rm sp} \sim (c/c^*)^1$ following the theoretical predictions.³⁸ For $c>c^*$, $\eta_{\rm sp}$ scales with polymer concentration as $\eta_{\rm sp}\sim(c/c^*)^{1/2}$ at low (10⁻⁶ M) and $\eta_{\rm sp} \sim (c/c^*)^{5/4}$ at high (10⁻¹ M) ionic strength, in accordance with predictions for polyelectrolytes. 16,38,49,50,52 For an intermediate ionic strength of 10^{-3} M, $\eta_{\rm sp} \sim (c/c^*)^{\alpha}$ with an exponent $\alpha = 0.8 \pm 0.1$ that falls between those found in the limits of low and high ionic strength. At a fixed c/c^* , $\eta_{\rm sp}$ increases concomitant with ionic strength, due to the increased chain-chain interactions as the salt screens the electrostatic interactions between ionized groups. 52 For 10^{-6} and 10^{-3} M solutions, the scaling exponents of $\eta_{\rm sp}$ are constant across the studied range of polymer concentrations, suggesting the absence of chain entanglements. For 10^{-1} M solutions, however, we observe an upturn in $\eta_{\rm sp}$ at high concentrations, which signals the presence of entanglements. These observations are consistent with expectations for the entanglements in charged polymer solutions. 50,52 Thus, the rheology measurements confirm that the conformation of the polyelectrolytes can be modified by screening the electrostatic interactions.

Using PSS with two different molecular weights of 68 and 2200 kDa at various ionic strengths and polymer concentrations, we tune polymer length scales ξ and $R_{\rm g}$ over a range that spans from the M13 phage diameter 2R to larger than the hydrodynamic radius of the phage $R_{\rm h}$ with different degrees of chain flexibility (Fig. 2). In 68 kDa PSS solutions, the phage diameter 2R and hydrodynamic radius $R_{\rm h}$ are comparable to and larger than the polymer size, respectively. For 2200 kDa PSS solutions, however, the phage diameter 2R is smaller than and the hydrodynamic radius $R_{\rm h}$ is comparable to the characteristic lengths of the polymer solutions (ξ , $R_{\rm g}$). In both cases, the length of the phage $L\approx 900$ nm is much larger than the polymer characteristic length scales. These comparisons indicate that PSS solutions are promising model systems in which to examine how dynamics of viruses depend

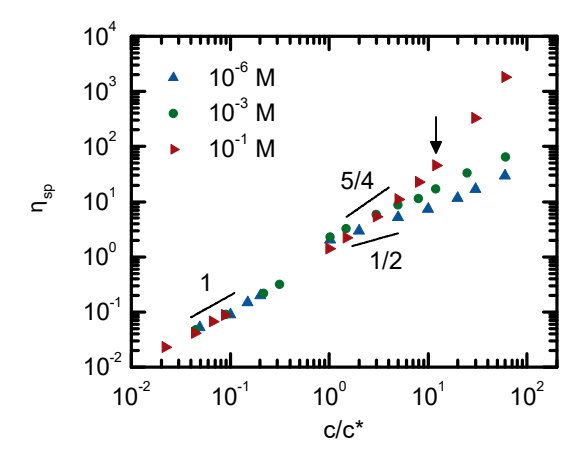


Figure 1: Specific viscosity $\eta_{\rm sp}=(\eta-\eta_0)/\eta_0$ as a function of normalized polymer concentration c/c^* for solutions of 2200 kDa PSS with various ionic strengths. The arrow points to the onset of entanglements in 10^{-1} M PSS solutions. Solid lines represent theoretical scaling in the limits of low and high ionic strength. ⁵²

on polymer length scales.

In the absence of polymer, the ensemble-averaged mean-squared displacements (MSDs) of M13 phage in aqueous electrolyte solutions with ionic strength of 10^{-6} , 10^{-3} , and 10^{-1} M increase linearly as a function of lag time Δt (Fig. 3). The long-time translational diffusivities D_0 , calculated from linear fits of the MSDs on long time scales, are 2.10 ± 0.12 , 2.11 ± 0.09 , and $2.15 \pm 0.06 \ \mu\text{m}^2\,\text{s}^{-1}$ for solutions with ionic strength of 10^{-6} , 10^{-3} , and 10^{-1} M, respectively. The measured values are in good agreement with previously reported diffusivities for M13 bacteriophage 43,53,54 and the structurally-identical fd virus. 55 The cor-

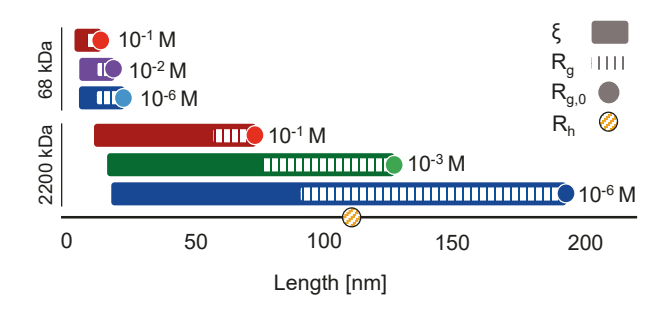


Figure 2: Schematic of length scales (solution correlation length ξ , polymer radius of gyration $R_{\rm g}$, polymer radius of gyration at infinite dilution $R_{\rm g,0}$, and phage hydrodynamic radius $R_{\rm h}$) in suspensions of M13 phage in 68 and 2200 kDa PSS polymer solutions at various concentrations and ionic strengths.

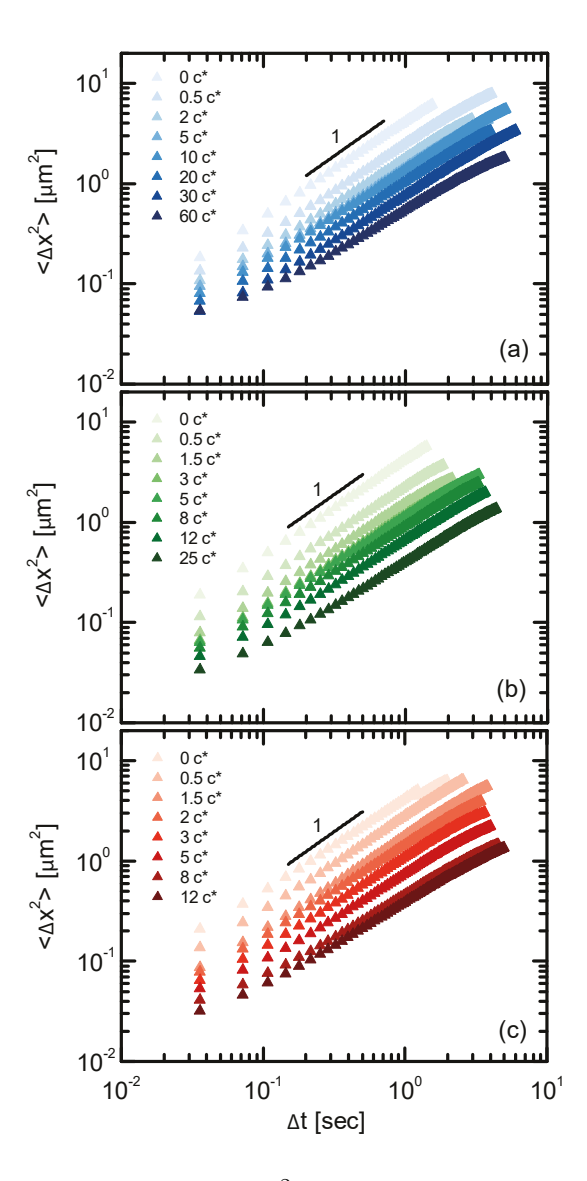


Figure 3: Mean-squared displacement $\langle \Delta x^2 \rangle$ as a function of lag time Δt for M13 bacteriophage for solutions with various concentration of 2200 kDa PSS and ionic strength of (a) 10^{-6} M, (b) 10^{-3} M, and (c) 10^{-1} M. Solid lines represent linear scaling.

responding hydrodynamic radii, calculated using the SE relationship, are 108 ± 6 , 107 ± 5 , and 105 ± 3 nm at 10^{-6} , 10^{-3} , and 10^{-1} M ionic strength, respectively. Although the net charge on the virus surface is negative, increasing the ionic strength and hence electrostatic screening does not markedly alter its hydrodynamic radius in pure electrolyte solutions. The hydrodynamic radii of M13 phage particles in electrolyte solutions are significantly smaller than the radius of gyration of rigid rods with similar dimensions (520 nm), confirming that

these filamentous viruses behave as semiflexible rods. 47

The MSDs of phage particles in solutions of 2200 kDa PSS also evolve linearly as a function of lag time Δt , indicating diffusive dynamics for all concentrations of polymer (Fig. 3). For a fixed solution ionic strength, the phage dynamics slow upon increasing the polymer concentration. Likewise, at a fixed polymer concentration c/c^* , the phage diffuse more slowly as the ionic strength increases (Fig. 4 (a)). Similar slowing of phage diffusive dynamics are also observed in solutions of 68 kDa PSS as either ionic strength or polymer concentration is increased (Fig. S6 and Fig. S7, Supporting Information). The slowing of the phage dynamics with increasing polymer concentration reflects the increased crowding in the solutions. Similarly, the slowing of phage dynamics with increasing ionic strength also reflects an increase in crowding, due to a change in the polymer size. Increasing the ionic strength suppresses electrostatic repulsions and the chains adopt a more collapsed conformation. This transition from an extended random walk to a Gaussian conformation increases the number density of the chains in a specific volume at a similar overlap concentration c^* , leading to increased crowding and hence slowing of the phage dynamics.

To assess how anisotropy affects the dynamics of the phage particles, we compare the diffusion coefficients of the phage with those of 100 nm radius PS nanospheres with similar hydrodynamic radius. The normalized diffusivity of the nanospheres decreases as either polymer concentration is increased or ionic strength is decreased (Fig. 4(a)). For a particular polymer concentration and ionic strength, however, the diffusivity of phage is greater than that of the nanospheres with similar hydrodynamic radius. This observation is consistent with the results of earlier studies showing that rod-like particles can exhibit higher diffusivity than their spherical counterparts. $^{57-60}$ Further, both phage and nanospheres dynamics differently depend on polymer concentration at low ionic strength compared to high ionic strength. The diffusion curves for solutions with ionic strength 10^{-6} and 10^{-3} M exhibit an inflection point at intermediate polymer concentrations, but decline approximately linearly with polymer concentration for an ionic strength of 10^{-1} M.

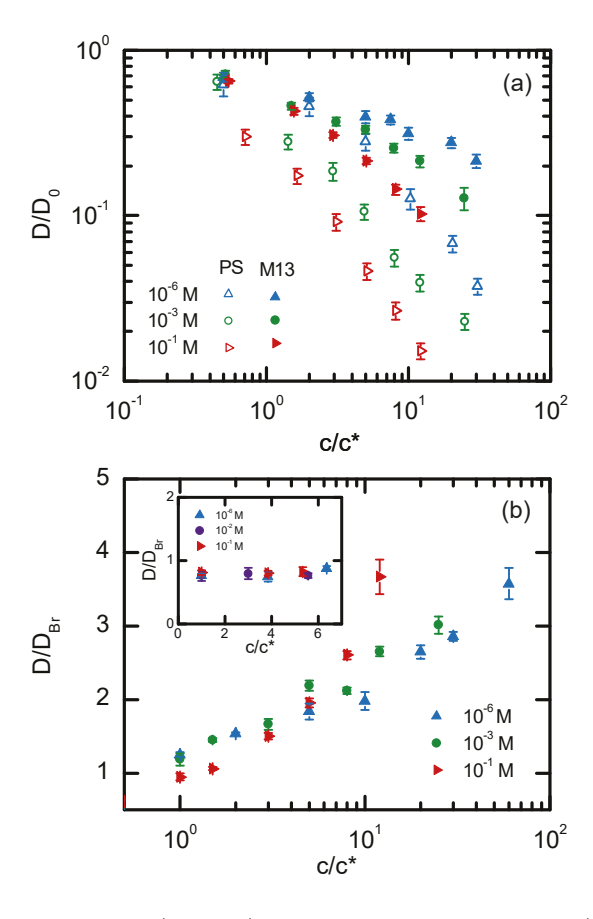


Figure 4: (a) Normalized phage (closed) and PS nanoparticles (open) diffusivity D/D_0 as a function of normalized polymer concentration c/c^* in solutions of 2200 kDa PSS with various ionic strengths. (b) Phage diffusivity normalized to Broersma's prediction 56 $D/D_{\rm Br}$ as a function of c/c^* in solutions of 2200 kDa PSS with various ionic strengths. Inset: Phage diffusivity normalized to Broersma's prediction 56 $D/D_{\rm Br}$ as a function of c/c^* in solutions of 68 kDa PSS with various ionic strengths. Error bars represent the standard deviation of four measurements per sample.

To test whether the faster phage dynamics arises from deviations from the bulk Stokes-Einstein prediction, we examine the phage diffusivity normalized by the Broersma diffusivity $D/D_{\rm Br}$ (Fig. 4 (b)). The Broersma model ^{56,61,62} is a hydrodynamic model based on the SE relationship used to predict the diffusivity of high aspect ratio rods from the bulk zero-shear-rate viscosity of the solution. ^{55,63-65} The model supplements the SE relationship with stick boundary conditions and treats the rods as diffusing in a homogeneous viscous medium with the derived diffusivity $D_{\rm Br} = (k_{\rm B}T/3\pi\eta L)[\delta - 1/2(\gamma_{\parallel} + \gamma_{\perp})]$ where δ , γ_{\parallel} , and γ_{\perp} are given in the Supporting Information (Rod diffusion model). For 68 kDa PSS solutions,

for which the polymer radii of gyration at finite dilution are smaller than phage length scales $(R_{\rm g,0} < 2R < L)$, $D/D_{\rm Br} \approx 0.9$ is independent of the polymer concentration within error (Fig. 4 (b) (inset)). The measured diffusivity is slightly lower than predicted (i.e. $D/D_{\rm Br} < 1$), which can be attributed to the presence of undetectable small aggregates of phage in the samples. For 2200 kDa PSS solutions near the overlap concentration $(c/c^* \approx 1)$, the relative diffusivities are in good agreement with the prediction of the Broersma model. As concentration increases, however, the normalized diffusivities increasingly deviate from the bulk prediction (Fig. 4 (b)). For this polymer, the phage diameter and length are smaller and larger than the polymer radius of gyration $(2R < R_{\rm g,0} < L)$, respectively. For systems with such relative length scales, the particle-polymer chain interactions become more important and result in a breakdown of the continuum assumption as reported for nanospheres 32,66,67 and nanorods. 17,18,21,46 These deviations confirm that M13 diffusion in charged polymer solutions cannot be described by models for rods in a homogeneous medium, and thus indicate that the phage diffusivity depends on polymer length scales.

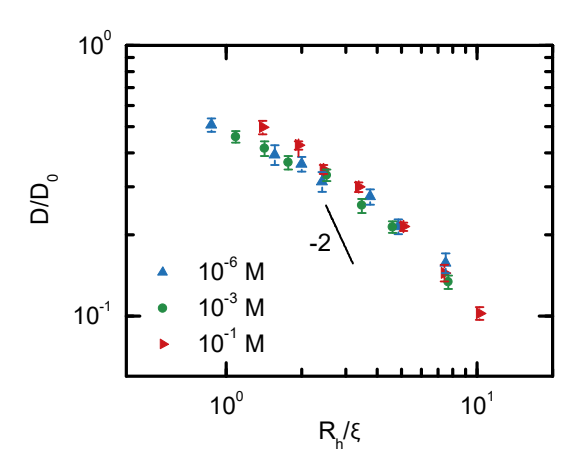


Figure 5: Normalized phage diffusivity D/D_0 as a function of M13 phage hydrodynamic radius to polymer size ratio $R_{\rm h}/\xi$ in semidilute $(c>c^*)$ solutions of 2200 kDa PSS with various ionic strengths. The $R_{\rm h}$ values calculated using the SE equation are 108 ± 6 , 107 ± 5 , and 105 ± 3 nm at 10^{-6} , 10^{-3} , and 10^{-1} M ionic strength, respectively. Error bars represent the standard deviation of four measurements per sample. Solid line represents theoretical scaling from the coupling theory.³²

The increasing deviation from the continuum model prediction as polymer concentration

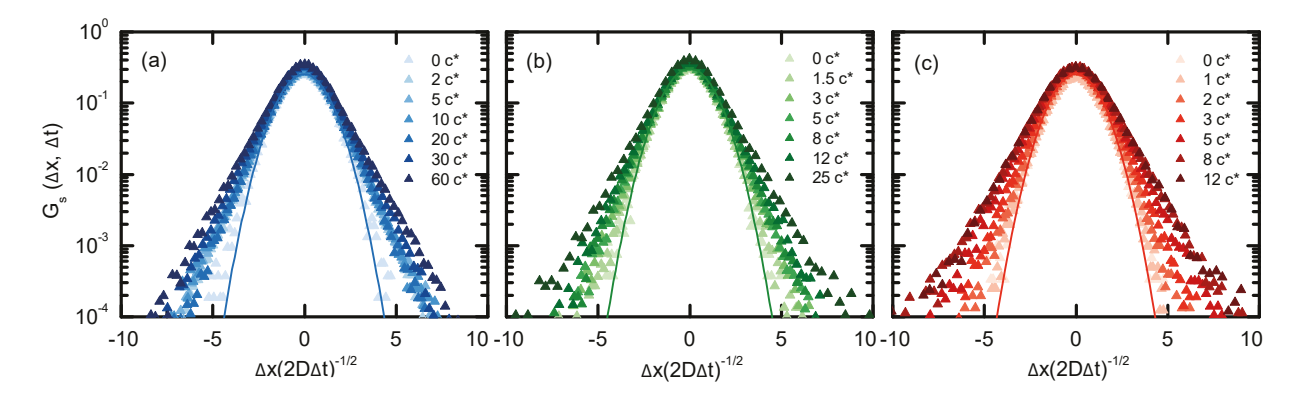


Figure 6: Normalized probability distribution of displacements $G_s(\Delta x, \Delta t)$ as a function of normalized displacement $\Delta x (2D\Delta t)^{-1/2}$ at $\Delta t = 0.036$ s for M13 bacteriophage in solutions of 2200 kDa PSS with various polymer concentrations at (a) 10^{-6} M, (b) 10^{-3} M, and (c) 10^{-1} M ionic strength. The solid curves indicate Gaussian predictions.

increases is qualitatively consistent with the predictions of mode coupling theory (MCT) proposed by Ref. 67. In this theory, the long-time diffusion coefficient of the particles is a sum of hydrodynamic and non-hydrodynamic contributions $D = D_{\text{hydro}} + D_{\text{non-hydro}}$, where D_{hydro} is determined by the bulk viscosity of the solution η and $D_{\text{non-hydro}}$ arises from the coupling of the particle motion to polymer structural relaxations. For short polymer chains with $R_{\text{NP}} > R_{\text{g,0}}$, MCT predicts that the hydrodynamic contribution is the dominant contribution to D. As the chain length increases, however, the non-hydrodynamic contribution becomes comparable to the hydrodynamic term, resulting in decoupling from the bulk viscosity prediction for $R_{\text{NP}} > R_{\text{g,0}}$, where the continuum assumption is expected to hold according to Ref. 67. For this size limit, MCT predicts that the non-hydrodynamic term further dominates the hydrodynamic contribution as the polymer crowding increases. This explanation is in good agreement with a recent simulation study of nanorods in polymer melts, ⁴⁶ which showed that hydrodynamic interactions are partially screened for melts of longer chains but are not screened for shorter chains.

To explain the deviations from the bulk prediction, we test the applicability of the coupling theory of Ref. 32. In the size regime $\xi < R_{\rm NP} < d_{\rm t}$, where $d_{\rm t}$ is the tube diameter of the polymer, this model predicts that the dynamics of particles decouple from the relaxation

modes of the polymer and instead are coupled to the relaxations of polymer chain segments of comparable size. As a result of this coupling, particles experience a lower effective viscosity and diffuse faster. For isotropic probes, this coupling is controlled by the particle size, resulting in $D/D_0 \sim (2R_{\rm NP}/\xi)^{-2}$ scaling in this size regime.³² By contrast, anisotropic particles have multiple length scales and it is not clear which of these control the particle diffusivity. In our previous study, 43 we showed that the dynamics of anisotropic viruses with various aspect ratios are controlled by effective length scales that are intermediate between the length L and diameter 2R of the viruses. In this study, however, the virus length scales are approximately constant as a function of salt concentration as shown by similar hydrodynamic radii R_h at various ionic strengths. Hence, we adopt the hydrodynamic radius as the phage characteristic length scale and test whether the phage normalized diffusivity D/D_0 can be scaled by R_h/ξ (Fig. 5). This scaling approximately collapses D/D_0 over the range of polymer length scales investigated with a slight bifurcation at low normalized concentrations, where the normalized diffusivities of the phage for 10^{-1} M solution are slightly greater than those for 10^{-3} and 10^{-6} M. The scaling behavior, however, is not in accordance with the $D/D_0 \sim (2R_{\rm NP}/\xi)^{-2}$ scaling predicted in Ref. 32.

Because this theory was developed for diffusion of nanospheres in neutral polymers, we hypothesize that the anisotropy of the probe particles or/and differences in the structure of PSS at various ionic strengths make this scaling theory unable to fully predict the dynamics of the system. To test our hypothesis, we examine the normalized diffusivity of the 100 nm PS particles (Fig. S9, Supporting Information). For 100 nm nanospheres, this scaling collapses the data onto a master curve following $D/D_0 \sim (2R_{\rm NP}/\xi)^{-2}$, as predicted by Ref. 32. Therefore, we conclude that in the range of length scales for which phage normalized diffusivities can be cleanly collapsed onto a single curve, anisotropy is the primary factor affecting the dynamical coupling of the phage and polymers controlled by the segmental relaxations of the polymer chains. At low normalized length scales (more dilute solutions), however, the phage likely probe the heterogeneities in charged polymers that exist over

length scales where the particles are similarly sized to the the polymer length scales ($R_{\rm g}$ and ξ). ⁶⁸ The structure of these heterogeneities, mediated by the electrostatic repulsion between monomers, are dictated by different polymer chain dynamics and relaxations at each ionic strength. ⁴¹

To explore how the anisotropic shape of the phage affects their coupling to the polymer dynamics, we calculate the probability distribution of displacements (PDDs) of the phage particles. To remove the concentration dependence, we normalize the displacement Δx by the diffusive displacement obtained from the finite diffusion coefficient at lag time Δt , $(2D\Delta t)^{1/2}$. For 68 kDa PSS, the PDDs are approximately Gaussian across all ionic strengths, as expected for Fickian diffusion (Fig. S8, Supporting Information). The PDDs of phage particles in 2200 kDa PSS, however, are non-Gaussian across all ionic strengths (Fig. 6). For a given ionic strength, the extent of deviation from the Gaussian prediction increases as c/c^* is increased, revealing higher probability of larger displacements. Likewise, for a fixed c/c^* , the non-Gaussianity of the PDDs is enhanced as the flexibility of the chains is increased (i.e., at higher ionic strengths). The transition from near-Gaussian distributions for the 68 kDa polymer to non-Gaussian distributions for the 2200 kDa polymer indicates that phage hydrodynamic interactions with polymer chains are affected by polymer length scales.

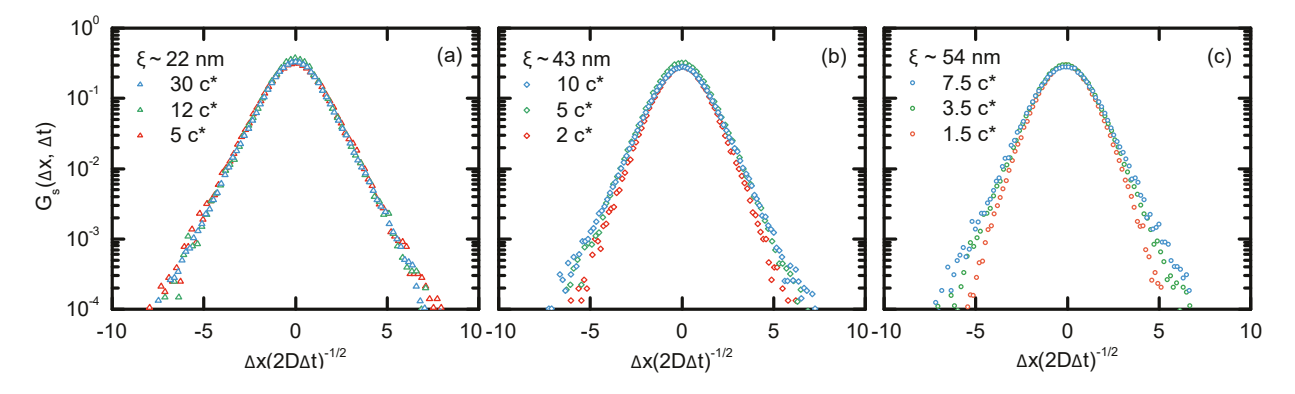


Figure 7: Normalized probability distribution of displacements $G_s(\Delta x, \Delta t)$ as a function of normalized displacement $\Delta x (2D\Delta t)^{-1/2}$ for M13 bacteriophage in solutions of various PSS concentrations and ionic strengths with approximate correlation length ξ of (a) 22, (b) 43, and (c) 54 nm. The lag time and polymer molecular weight are $\Delta t = 0.036$ s and $M_w = 2200$ kDa, respectively.

Non-Gaussian displacement distributions are attributed to a distribution of diffusivities ^{69,70} and/or diffusing diffusivity ⁷¹ in a system as particles experience a locally heterogeneous environment; 16,72 to anisotropic hydrodynamic interactions with the medium; 43,73 or to hopping between transient cages in matrices. ^{68,74} In our earlier study on dynamics of nanospheres in PSS solutions, we found that the distinctive structural properties of polyelectrolytes leads to the emergence of local heterogeneities in the system, resulting in non-Gaussian dynamics. 16 This behavior, however, is only observed in limited ranges of concentration $(c/c^* \approx 1-20)$ at the lowest ionic strength (10^{-6} M) and thus cannot completely explain the non-Gaussian phage dynamics observed at all salt and polymer concentrations. Moreover, the ergodicity breaking parameter EB is close to the Brownian motion limit and the non-Gaussian parameter α_2 exhibits fairly small values for all the polymer concentrations and ionic strengths (Fig. S10 and Fig. S11, Supporting Information). Furthermore, the PSS solutions are not entangled in our experiments except for $c/c^* = 12$ at 10^{-1} M solutions, indicating that intermittent hopping within the mesh does not explain the non-Gaussian behavior. Instead, in analogy with a physical picture developed for nanosphere diffusion in polymer matrices,²² we propose that in a specific size range, the anisotropy of the filamentous viruses results in different degrees of particle-polymer coupling for viruses moving along or normal to their main axis and thus leads to the emergence of non-Gaussian dynamics. For diffusion of isotropic particles sufficiently larger than the polymer characteristic size, the relaxation of the entire chain is required. For smaller particles, however, diffusion is controlled by the local relaxation of chain segments. In support of this picture, for 68 kDa PSS solutions whose characteristic sizes are smaller than the characteristic size of the virus, phage explore a homogeneous environment, couple to the relaxation of the polymer chains (Fig. 4 (b) (inset)), and exhibit Gaussian dynamics (Fig. S5, Supporting Information). For 2200 kDa PSS solutions whose size is bigger than the phage diameter 2R and much smaller than the phage length L, however, phage experience different hydrodynamic interactions moving along or normal to their main axis. We posit that the entire chain must relax for phage to diffuse normal to their major axis, whereas local segmental relaxations control diffusion along their major axis. These different degrees of phage-polymer coupling in each of these modes result in distinct distributions of diffusivities and non-Gaussian dynamics.

The collapse of the phage diffusivities with a normalized length scale suggests that the primary factor controlling the dynamics is the structural length scale ξ . To evaluate the relationship between the phage dynamics and the polymer structure, we compare the displacement distributions of the phage particles in PSS solutions of different ionic strength and similar ξ (Fig. 7). For $\xi \approx 22$ nm, where the normalized diffusivities are nearly equal for all three ionic strengths (Fig. 5), the PDDs collapse onto a single curve (Fig. 7(a)), confirming that the phage dynamics are controlled by the relaxations of polymer segments of comparable size in this regime. For the intermediate correlation length $\xi \approx 43$ nm at which the diffusivities of phage in the 10^{-1} M solution begin to deviate from those in the other solutions (Fig. 5), however, the PDD curves do not cleanly collapse. Instead, the PDD for the 10^{-1} M solution is slightly narrower than those for 10^{-3} and 10^{-6} M (Fig. 7 (b)). For a higher correlation length $\xi \approx 54$ nm, where the normalized diffusivities of the phage in 10^{-1} M solution are higher than those in the other solutions (Fig. 5), the PDD curves clearly separate from each other (Fig. 7(c)). Thus, we observe excellent agreement between the controlling physics obtained from the normalized diffusivities and the PDDs at matched characteristic length scales. Together, these results suggest that the anisotropy of phage and unique structural properties of PSS solutions affect the dynamic coupling of the phage and charged polymers.

Conclusions

We probe the dynamics of filamentous M13 phage as a model semiflexible nanorod in semidilute solutions of sodium polystyrene sulfonate (2200 kDa and 68 kDa), at various ionic strengths ranging from 10^{-6} to 10^{-1} M. Phage exhibit Fickian diffusion in all the solutions

with dynamics that slow upon increasing the polymer concentration and ionic strength. For 68 kDa PSS solutions ($R_{\rm g,0} < 2R < L$), phage diffuse according to the bulk viscosity (Broersma) predictions at all ionic strengths and exhibit Gaussian distributions of displacements. In 2200 kDa PSS solutions ($2R < R_{\rm g,0} < L$), however, the phage dynamics monotonically deviate from the bulk prediction and exhibit non-Gaussian distribution of displacements as concentration increases. The faster-than-expected diffusivities can approximately be collapsed onto a single curve as a function of the relative length scales $R_{\rm h}/\xi$ of the system. The partial collapse, however, does not follow the scaling prediction for diffusion of isotropic particles in solutions of the fully flexible Gaussian chains. We suggest that anisotropy of the phage and the unique structural properties of charged polymers are responsible for distinct length-dependent coupling of the phage diffusion and polyelectrolyte solutions.

The role of the particle shape and polymer architecture is not yet included in existing theoretical models;⁷⁵ our experiments and future studies are expected to inspire new theories. We anticipate that bacteriophage can serve as useful anisotropic model particles for probing the scale-dependent viscoelasticity or local heterogeneity in biological systems.^{34,76} More broadly, improved understanding of phage dynamics may benefit applications requiring control over diffusion of anisotropic particles in complex media such as biological gels,⁷⁷ cytoskeletal networks,⁷⁸ fibrous media,⁷⁹ and suspensions of rods.⁸⁰

Acknowledgement

We thank Prof. Megan Robertson for access to the rheometer. This work was supported by NSF (CBET-2004652, CBET-2113769) and the Welch Foundation (E-1869).

Supporting Information Available

Supporting Information contains intrinsic viscosity, polymer length scales, rod diffusion model, rheology, supplementary diffusivity plots, phage dynamics in 68 kDa PSS solutions, scaling model for nanospheres, ergodicity breaking parameter, non-Gaussian parameter, pH of the polymer solutions, and zeta potential of nanoparticles.

References

- (1) Sidhu, S. S. Engineering M13 for phage display. *Biomolecular engineering* **2001**, *18*, 57–63.
- (2) Lee, C. M.; Iorno, N.; Sierro, F.; Christ, D. Selection of human antibody fragments by phage display. *Nature protocols* **2007**, *2*, 3001–3008.
- (3) Flynn, C. E.; Lee, S.-W.; Peelle, B. R.; Belcher, A. M. Viruses as vehicles for growth, organization and assembly of materials. *Acta Materialia* **2003**, *51*, 5867–5880.
- (4) Clark, J. R.; March, J. B. Bacteriophages and biotechnology: vaccines, gene therapy and antibacterials. *Trends in biotechnology* **2006**, *24*, 212–218.
- (5) Matsuzaki, S.; Rashel, M.; Uchiyama, J.; Sakurai, S.; Ujihara, T.; Kuroda, M.; Ikeuchi, M.; Tani, T.; Fujieda, M.; Wakiguchi, H., et al. Bacteriophage therapy: a revitalized therapy against bacterial infectious diseases. *Journal of infection and chemother-apy* 2005, 11, 211–219.
- (6) Golkar, Z.; Bagasra, O.; Pace, D. G. Bacteriophage therapy: a potential solution for the antibiotic resistance crisis. The Journal of Infection in Developing Countries 2014, 8, 129–136.
- (7) Nanduri, V.; Sorokulova, I. B.; Samoylov, A. M.; Simonian, A. L.; Petrenko, V. A.;

- Vodyanoy, V. Phage as a molecular recognition element in biosensors immobilized by physical adsorption. *Biosensors and Bioelectronics* **2007**, *22*, 986–992.
- (8) Riseman, J.; Kirkwood, J. G. The intrinsic viscosity, translational and rotatory diffusion constants of rod-like macromolecules in solution. *The Journal of Chemical Physics* **1950**, *18*, 512–516.
- (9) Ye, X.; Tong, P.; Fetters, L. Transport of probe particles in semidilute polymer solutions. *Macromolecules* **1998**, *31*, 5785–5793.
- (10) Cheng, Y.; Prud'Homme, R. K.; Thomas, J. L. Diffusion of mesoscopic probes in aqueous polymer solutions measured by fluorescence recovery after photobleaching. *Macro-molecules* 2002, 35, 8111–8121.
- (11) Mackay, M. E.; Dao, T. T.; Tuteja, A.; Ho, D. L.; Van Horn, B.; Kim, H.-C.; Hawker, C. J. Nanoscale effects leading to non-Einstein-like decrease in viscosity. *Nature materials* 2003, 2, 762–766.
- (12) Tuteja, A.; Mackay, M. E.; Narayanan, S.; Asokan, S.; Wong, M. S. Breakdown of the continuum Stokes- Einstein relation for nanoparticle diffusion. *Nano letters* 2007, 7, 1276–1281.
- (13) Poling-Skutvik, R.; Krishnamoorti, R.; Conrad, J. C. Size-dependent dynamics of nanoparticles in unentangled polyelectrolyte solutions. ACS Macro Letters 2015, 4, 1169–1173.
- (14) Chen, R.; Poling-Skutvik, R.; Nikoubashman, A.; Howard, M. P.; Conrad, J. C.; Palmer, J. C. Coupling of nanoparticle dynamics to polymer center-of-mass motion in semidilute polymer solutions. *Macromolecules* 2018, 51, 1865–1872.
- (15) Chen, R.; Poling-Skutvik, R.; Howard, M. P.; Nikoubashman, A.; Egorov, S. A.; Con-

- rad, J. C.; Palmer, J. C. Influence of polymer flexibility on nanoparticle dynamics in semidilute solutions. *Soft Matter* **2019**, *15*, 1260–1268.
- (16) Slim, A. H.; Poling-Skutvik, R.; Conrad, J. C. Local confinement controls diffusive nanoparticle dynamics in semidilute polyelectrolyte solutions. *Langmuir* 2020, 36, 9153–9159.
- (17) Alam, S.; Mukhopadhyay, A. Translational and rotational diffusions of nanorods within semidilute and entangled polymer solutions. *Macromolecules* **2014**, *47*, 6919–6924.
- (18) Choi, J.; Cargnello, M.; Murray, C. B.; Clarke, N.; Winey, K. I.; Composto, R. J. Fast nanorod diffusion through entangled polymer melts. *ACS Macro Letters* **2015**, *4*, 952–956.
- (19) Lee, J.; Grein-Iankovski, A.; Narayanan, S.; Leheny, R. L. Nanorod mobility within entangled wormlike micelle solutions. *Macromolecules* **2017**, *50*, 406–415.
- (20) Li, S.-J.; Qian, H.-J.; Lu, Z.-Y. Translational and rotational dynamics of an ultra-thin nanorod probe particle in linear polymer melts. *Physical Chemistry Chemical Physics* **2018**, *20*, 20996–21007.
- (21) Karatrantos, A.; Composto, R. J.; Winey, K. I.; Clarke, N. Nanorod diffusion in polymer nanocomposites by molecular dynamics simulations. *Macromolecules* **2019**, *52*, 2513–2520.
- (22) Wyart, F. B.; de Gennes, P.-G. Viscosity at small scales in polymer melts. *The European Physical Journal E* **2000**, *1*, 93–97.
- (23) Guo, H.; Bourret, G.; Lennox, R. B.; Sutton, M.; Harden, J. L.; Leheny, R. L. Entanglement-controlled subdiffusion of nanoparticles within concentrated polymer solutions. *Physical Review Letters* 2012, 109, 055901.

- (24) Kalathi, J. T.; Yamamoto, U.; Schweizer, K. S.; Grest, G. S.; Kumar, S. K. Nanoparticle diffusion in polymer nanocomposites. *Physical review letters* **2014**, *112*, 108301.
- (25) Yamamoto, U.; Schweizer, K. S. Microscopic theory of the long-time diffusivity and intermediate-time anomalous transport of a nanoparticle in polymer melts. *Macro-molecules* **2015**, *48*, 152–163.
- (26) Ogston, A. G.; Preston, B.; Wells, J. On the transport of compact particles through solutions of chain-polymers. *Proceedings of the Royal Society of London. A. Mathematical and Physical Sciences* **1973**, *333*, 297–316.
- (27) Johansson, L.; Elvingson, C.; Loefroth, J. E. Diffusion and interaction in gels and solutions. 3. Theoretical results on the obstruction effect. *Macromolecules* 1991, 24, 6024–6029.
- (28) Cukier, R. Diffusion of Brownian spheres in semidilute polymer solutions. *Macro-molecules* **1984**, *17*, 252–255.
- (29) Phillies, G. D. Universal scaling equation for self-diffusion by macromolecules in solution. *Macromolecules* **1986**, *19*, 2367–2376.
- (30) Altenberger, A. R.; Tirrell, M.; Dahler, J. S. Hydrodynamic screening and particle dynamics in porous media, semidilute polymer solutions and polymer gels. *The Journal* of chemical physics 1986, 84, 5122–5130.
- (31) Fujita, H. Fortschritte Der Hochpolymeren-Forschung; Springer, 1961; pp 1–47.
- (32) Cai, L.-H.; Panyukov, S.; Rubinstein, M. Mobility of spherical probe objects in polymer liquids. *Macromolecules* **2011**, *44*, 7853–7863.
- (33) Tsay, J. M.; Doose, S.; Weiss, S. Rotational and translational diffusion of peptide-coated CdSe/CdS/ZnS nanorods studied by fluorescence correlation spectroscopy. *Journal of the American Chemical Society* **2006**, *128*, 1639–1647.

- (34) Molaei, M.; Atefi, E.; Crocker, J. C. Nanoscale rheology and anisotropic diffusion using single gold nanorod probes. *Physical review letters* **2018**, *120*, 118002.
- (35) De Gennes, P.-G.; Pincus, P.; Velasco, R.; Brochard, F. Remarks on polyelectrolyte conformation. *Journal de physique* **1976**, *37*, 1461–1473.
- (36) De Gennes, P.-G.; Gennes, P.-G. Scaling concepts in polymer physics; Cornell university press, 1979.
- (37) Pfeuty, P. Conformation des polyelectrolytes ordre dans les solutions de polyelectrolytes.

 Le Journal de Physique Colloques 1978, 39, C2–149.
- (38) Dobrynin, A. V.; Colby, R. H.; Rubinstein, M. Scaling theory of polyelectrolyte solutions. *Macromolecules* **1995**, *28*, 1859–1871.
- (39) Carrillo, J.-M. Y.; Dobrynin, A. V. Polyelectrolytes in salt solutions: Molecular dynamics simulations. *Macromolecules* **2011**, *44*, 5798–5816.
- (40) Muthukumar, M. 50th anniversary perspective: A perspective on polyelectrolyte solutions. *Macromolecules* **2017**, *50*, 9528–9560.
- (41) Slim, A. H.; Shi, W. H.; Safi Samghabadi, F.; Faraone, A.; Marciel, A. B.; Poling-Skutvik, R.; Conrad, J. C. Electrostatic Repulsion Slows Relaxations of Polyelectrolytes in Semidilute Solutions. ACS Macro Letters 2022, 11, 854–860.
- (42) Cush, R.; Russo, P. S.; Kucukyavuz, Z.; Bu, Z.; Neau, D.; Shih, D.; Kucukyavuz, S.; Ricks, H. Rotational and translational diffusion of a rodlike virus in random coil polymer solutions. *Macromolecules* **1997**, *30*, 4920–4926.
- (43) Smith, M.; Poling-Skutvik, R.; Slim, A. H.; Willson, R. C.; Conrad, J. C. Dynamics of Flexible Viruses in Polymer Solutions. *Macromolecules* **2021**, *54*, 4557–4563.

- (44) Lee, K. L.; Hubbard, L. C.; Hern, S.; Yildiz, I.; Gratzl, M.; Steinmetz, N. F. Shape matters: the diffusion rates of TMV rods and CPMV icosahedrons in a spheroid model of extracellular matrix are distinct. *Biomaterials science* **2013**, *1*, 581–588.
- (45) Schweizerhof, S.; Demco, D. E.; Mourran, A.; Fechete, R.; Moller, M. Diffusion of gold nanorods functionalized with thermoresponsive polymer brushes. *Langmuir* **2018**, *34*, 8031–8041.
- (46) Wang, J.; O'Connor, T. C.; Grest, G. S.; Zheng, Y.; Rubinstein, M.; Ge, T. Diffusion of Thin Nanorods in Polymer Melts. *Macromolecules* **2021**, *54*, 7051–7059.
- (47) Song, L.; Kim, U.-S.; Wilcoxon, J.; Schurr, J. M. Dynamic light scattering from weakly bending rods: estimation of the dynamic bending rigidity of the M13 virus. *Biopolymers: Original Research on Biomolecules* **1991**, *31*, 547–567.
- (48) Cohen, J.; Priel, Z.; Rabin, Y. Viscosity of dilute polyelectrolyte solutions. *The Journal of chemical physics* **1988**, *88*, 7111–7116.
- (49) Boris, D. C.; Colby, R. H. Rheology of sulfonated polystyrene solutions. *Macromolecules* 1998, 31, 5746–5755.
- (50) Lopez, C. G. Entanglement Properties of Polyelectrolytes in Salt-Free and Excess-Salt Solutions. ACS Macro Letters 2019, 8, 979–983.
- (51) Crocker, J. C.; Grier, D. G. Methods of digital video microscopy for colloidal studies.

 Journal of colloid and interface science 1996, 179, 298–310.
- (52) Colby, R. H. Structure and linear viscoelasticity of flexible polymer solutions: comparison of polyelectrolyte and neutral polymer solutions. *Rheologica acta* **2010**, *49*, 425–442.
- (53) Beck, K.; Duenk, R. M. Flexibility of bacteriophage M13: Comparison of hydrodynamic measurements with electron microscopy. *Journal of structural biology* **1990**, *105*, 22–27.

- (54) Song, L.; Kim, U.-S.; Wilcoxon, J.; Schurr, J. M. Dynamic light scattering from weakly bending rods: estimation of the dynamic bending rigidity of the M13 virus. *Biopolymers: Original Research on Biomolecules* **1991**, *31*, 547–567.
- (55) Maeda, T.; Fujime, S. Dynamic light-scattering study of suspensions of fd virus. Application of a theory of light-scattering spectrum of weakly bending filaments. *Macro-molecules* **1985**, *18*, 2430–2437.
- (56) Broersma, S. Rotational diffusion constant of a cylindrical particle. *The Journal of Chemical Physics* **1960**, *32*, 1626–1631.
- (57) Fakhri, N.; MacKintosh, F. C.; Lounis, B.; Cognet, L.; Pasquali, M. Brownian motion of stiff filaments in a crowded environment. *Science* **2010**, *330*, 1804–1807.
- (58) Chauhan, V. P.; Popović, Z.; Chen, O.; Cui, J.; Fukumura, D.; Bawendi, M. G.; Jain, R. K. Fluorescent nanorods and nanospheres for real-time in vivo probing of nanoparticle shape-dependent tumor penetration. *Angewandte Chemie* 2011, 123, 11619–11622.
- (59) Yu, M.; Wang, J.; Yang, Y.; Zhu, C.; Su, Q.; Guo, S.; Sun, J.; Gan, Y.; Shi, X.; Gao, H. Rotation-facilitated rapid transport of nanorods in mucosal tissues. *Nano Letters* 2016, 16, 7176–7182.
- (60) Wang, J.; Yang, Y.; Yu, M.; Hu, G.; Gan, Y.; Gao, H.; Shi, X. Diffusion of rod-like nanoparticles in non-adhesive and adhesive porous polymeric gels. *Journal of the Mechanics and Physics of Solids* **2018**, *112*, 431–457.
- (61) Broersma, S. Viscous force constant for a closed cylinder. The Journal of Chemical Physics 1960, 32, 1632–1635.
- (62) Broersma, S. Viscous force and torque constants for a cylinder. *The Journal of Chemical Physics* **1981**, *74*, 6989–6990.

- (63) Cush, R.; Russo, P. S.; Kucukyavuz, Z.; Bu, Z.; Neau, D.; Shih, D.; Kucukyavuz, S.; Ricks, H. Rotational and translational diffusion of a rodlike virus in random coil polymer solutions. *Macromolecules* **1997**, *30*, 4920–4926.
- (64) Su, C.-Y.; Yang, A.-C.; Jiang, J.-S.; Yang, Z.-H.; Huang, Y.-S.; Kang, D.-Y.; Hua, C.-C. Properties of single-walled aluminosilicate nanotube/poly (vinyl alcohol) aqueous dispersions. The Journal of Physical Chemistry B 2018, 122, 380–391.
- (65) Eichler-Volf, A.; Huang, T.; Vazquez Luna, F.; Alsaadawi, Y.; Stierle, S.; Cuniberti, G.; Steinhart, M.; Baraban, L.; Erbe, A. Comparative Studies of Light-Responsive Swimmers: Janus Nanorods versus Spherical Particles. *Langmuir* **2020**, *36*, 12504–12512.
- (66) Ziębacz, N.; Wieczorek, S. A.; Kalwarczyk, T.; Fiałkowski, M.; Hołyst, R. Crossover regime for the diffusion of nanoparticles in polyethylene glycol solutions: influence of the depletion layer. Soft Matter 2011, 7, 7181–7186.
- (67) Egorov, S. Anomalous nanoparticle diffusion in polymer solutions and melts: A mode-coupling theory study. *The Journal of chemical physics* **2011**, *134*, 084903.
- (68) Wong, I.; Gardel, M.; Reichman, D.; Weeks, E. R.; Valentine, M.; Bausch, A.; Weitz, D. A. Anomalous diffusion probes microstructure dynamics of entangled F-actin networks. *Physical review letters* 2004, 92, 178101.
- (69) Wang, B.; Anthony, S. M.; Bae, S. C.; Granick, S. Anomalous yet brownian. *Proceedings of the National Academy of Sciences* **2009**, *106*, 15160–15164.
- (70) Hapca, S.; Crawford, J. W.; Young, I. M. Anomalous diffusion of heterogeneous populations characterized by normal diffusion at the individual level. *Journal of the Royal Society Interface* **2009**, *6*, 111–122.
- (71) Chubynsky, M. V.; Slater, G. W. Diffusing diffusivity: a model for anomalous, yet Brownian, diffusion. *Physical review letters* **2014**, *113*, 098302.

- (72) He, W.; Song, H.; Su, Y.; Geng, L.; Ackerson, B. J.; Peng, H.; Tong, P. Dynamic heterogeneity and non-Gaussian statistics for acetylcholine receptors on live cell membrane.

 Nature communications 2016, 7, 1–8.
- (73) Han, Y.; Alsayed, A. M.; Nobili, M.; Zhang, J.; Lubensky, T. C.; Yodh, A. G. Brownian motion of an ellipsoid. *Science* **2006**, *314*, 626–630.
- (74) Lettinga, M. P.; Alvarez, L.; Korculanin, O.; Grelet, E. When bigger is faster: A self-Van Hove analysis of the enhanced self-diffusion of non-commensurate guest particles in smectics. The Journal of Chemical Physics 2021, 154, 204901.
- (75) Roosen-Runge, F.; Schurtenberger, P.; Stradner, A. Self-diffusion of nonspherical particles fundamentally conflicts with effective sphere models. *Journal of Physics: Condensed Matter* **2021**, *33*, 154002.
- (76) Nishi, K.; MacKintosh, F. C.; Schmidt, C. F. Multiscale Microrheology Using Fluctuating Filaments as Stealth Probes. *Physical Review Letters* **2021**, *127*, 158001.
- (77) Lee, B. J.; Cheema, Y.; Bader, S.; Duncan, G. A. Shaping nanoparticle diffusion through biological barriers to drug delivery. *JCIS Open* **2021**, 4, 100025.
- (78) Garamella, J.; Regan, K.; Aguirre, G.; McGorty, R. J.; Robertson-Anderson, R. M. Anomalous and heterogeneous DNA transport in biomimetic cytoskeleton networks. Soft Matter 2020, 16, 6344–6353.
- (79) Kim, J.; Vu, B.; Kourentzi, K.; Willson, R. C.; Conrad, J. C. Increasing binding efficiency via reporter shape and flux in a viral nanoparticle lateral-flow assay. *ACS applied materials & interfaces* **2017**, *9*, 6878–6884.
- (80) Abakumov, S.; Deschaume, O.; Bartic, C.; Lang, C.; Korculanin, O.; Dhont, J. K. G.; Lettinga, M. P. Uncovering Log Jamming in Semidilute Suspensions of Quasi-Ideal Rods. *Macromolecules* 2021, 54, 9609–9617.

Graphical TOC Entry

